Development of a One-Equation Transition / Turbulence Model

J. R. Edwards *
North Carolina State University, Raleigh, NC
C. J. Roy• †
Sandia National Laboratories, Albuquerque, NM
F. G. Blottner• ‡
Sandia National Laboratories, Albuquerque, NM
H. A. Hassan §
North Carolina State University, Raleigh, NC

August 1, 2000

Abstract

This paper reports on the development of a unified one-equation model for the prediction of transitional and turbulent flows. An eddy viscosity - transport equation for non-turbulent fluctuation growth based on that proposed by Warren and Hassan (*Journal of Aircraft*, Vol. 35, No. 5) is combined with the Spalart-Allmaras one-equation model for turbulent fluctuation growth. Blending of the two equations is accomplished through a multidimensional

*Associate Professor, Dept. of Mechanical and Aerospace Engineering, Campus Box 7910, NCSU, Raleigh, NC 27695; jredward@eos.ncsu.edu; (919) 515-5264; Senior Member AIAA

†Senior Member of Technical Staff, Thermal/Fluid Computational Engineering Sciences Department, Mail Stop 0835, P. O. Box 5800, Albuquerque, NM 87185-0835, Member AIAA

‡Distinguished Member of Technical Staff, Aerosciences and Compressible Fluid Mechanics Department, Mail Stop 0825, P. O. Box 5800, Albuquerque, NM 87185-0825, Fellow AIAA

§Professor, Dept. of Mechanical and Aerospace Engineering, Campus Box 7910, NCSU, Raleigh, NC 27695; hassan@eos.ncsu.edu; (919) 515-5241; Associate Fellow AIAA

• Sandia is a multiprogram laboratory operated by Sandia Corporation, a Lockheed Martin Company, for the United States Department of Energy under Contract DE-AC04-94AL85000

** Based on AIAA Paper 2000-0133, presented at the 31st Aerospace Sciences Meeting and Exhibit, Reno, NV

DISCLAIMER

intermittency function based on the work of Dhawan and Narasimha (*Journal of Fluid Mechanics,* Vol. 3, No. 4). The model predicts both the onset and extent of transition. Low-speed test cases include transitional flow over a flat plate, a single element airfoil, and a multi-element airfoil in landing configuration. High-speed test cases include transitional Mach 3.5 flow over a 5° cone and Mach 6 flow over a flared-cone configuration. Results are compared with experimental data, and the spatial accuracy of selected predictions is analyzed.

Nomenclature

a	=	model constant
b	=	model constant
C_{b_1}	=	Spalart-Allmaras model constant
C_μ	=	model constant
C_t	=	model constant
C_{t_3}	=	Spalart-Allmaras model constant
C_{t_4}	=	Spalart-Allmaras model constant
C_{w_1}	=	Spalart-Allmaras model constant
d	=	distance to nearest wall
f_{t_2}	=	transition function in Spalart-Allmaras model
f_{v_1}	=	wall damping function in Spalart-Allmaras model

f_w = wall blockage function in Spalart-Allmaras model

k = fluctuation kinetic energy

Re = Reynolds number

R_T = turbulence Reynolds number

s = surface distance

T = temperature

Tu = turbulence intensity (percentage)

γ = ratio of specific heats

Γ = intermittency function

δ = Boundary layer thickness

η = localization function

κ = von Karman constant

λ = relaxation length

ν = kinematic viscosity

ν_{nt} = "non-turbulent" eddy viscosity

$\tilde{\nu}$ = transported eddy viscosity in Spalart-Allmaras model

ϕ = flow property in Richardson Extrapolation

σ = model constant

τ = time scale

ξ	=	variable used in intermittency function
ζ	=	enstrophy (vorticity variance)
ω	=	characteristic frequency of disturbance
Ω	=	vorticity vector magnitude

subscripts

aw	=	adiabatic wall
b	=	boundary layer
e	=	boundary layer edge
l	=	laminar
nt	=	non-turbulent
N	=	Narasimha
o	=	stagnation conditions
t	=	transitional or turbulent
w	=	wall
∞	=	free stream conditions

superscripts

$*$	=	boundary layer reference state

Introduction

Earlier works[1–4] have detailed the development of a unified modeling approach for transitional / turbulent flows based on the combination of the $k - \zeta$ (enstrophy) turbulence model[5] with a model for non-turbulent fluctuation growth.[1, 2] Linear stability theory is used to guide the modeling of the non-turbulent fluctuation growth process which leads to transition. Thus far, Tollmien-Schlichting, crossflow, and second-mode mechanisms have been implemented into the model, with generally good results having been achieved for a variety of flowfields.

This paper reports on the application of these ideas to one-equation "eddy viscosity transport" turbulence models. Initial attention is focused on the popular Spalart-Allmaras one-equation model,[6] but the procedures as developed should be applicable to other models of this type. An eddy viscosity-transport model for non-turbulent fluctuation growth is proposed through analogy with the work of Warren and Hassan.[1, 2] Blending of this formulation with the fully-turbulent Spalart-Allmaras model is achieved through a multidimensional intermittency function based on the work of Dhawan and Narasimha.[7] The sections that follow present the unified one-equation transition / turbulence model and describe results that illustrate its effectiveness in simulating a variety of transitional flows.

Model Description

In the Warren-Hassan transition model, the growth of the non-turbulent fluctuation kinetic energy (k) is modeled by an equation of the following form:

$$\frac{Dk}{Dt} = \nu_{nt}\Omega(\Omega - (a+b)\frac{k}{\sqrt{2}\nu}) + \frac{\partial}{\partial x_j}((\frac{\nu}{3} + 1.8\nu_{nt})\frac{\partial k}{\partial x_j}), \tag{1}$$

where

$$\nu_{nt} = C_\mu k \tau_{nt}, \tag{2}$$

and Ω is the magnitude of the vorticity vector. The time scale τ_{nt} ("nt" for "non turbulent") is characteristic of the prevailing transition mechanism. The present work models transition due to both first and second-mode disturbances, thus

$$\tau_{nt} = \tau_{nt_1} + \tau_{nt_2}, \tag{3}$$

where the subscripts 1 and 2 refer to first- and second-mode contributions.

For first mode (Tollmein-Schlicting) transition,

$$\tau_{nt_1} = \frac{a}{\omega_1} \tag{4}$$

In this, ω_1 represents the frequency of the first-mode disturbance having the maximum amplification rate and is correlated as a function of surface distance s by the following:[3]

$$\frac{\omega_1 \nu_e}{U_e^2} = 0.48 Re_s^{-0.65} \tag{5}$$

Second-mode contributions are modeled as[3]

$$\tau_{nt_2} = \frac{b}{\omega_2}, \tag{6}$$

where

$$\omega_2 = 0.47 \frac{U_e}{\delta(s)} \tag{7}$$

and $\delta(s)$ is the boundary layer thickness.

In these descriptions, the subscript "e" represents an evaluation at the edge of the boundary layer. To account for compressibility effects, the kinematic viscosity ν_e in Eq. 5 is evaluated at a reference temperature T^*, defined as[3]

$$\frac{T^*}{T_e} = 1 + 0.032 M_e^2 + 0.56 (\frac{T_w}{T_e} - 1) \tag{8}$$

The calculation (or estimation) of edge quantities is a necessary, but somewhat cumbersome aspect of the transition model. The calculations presented later either determine them directly through a searching procedure (flat plate, supersonic cone, and hypersonic flared cone), or estimate them from the surface pressure distribution by assuming isentropic, adiabatic flow in the inviscid regions and zero pressure gradient in the direction normal to the surface (low-speed airfoils). The quantity s is a surface distance measured from the stagnation point. Other quantities appearing in the formulation include the magnitude of the vorticity vector Ω and the model constants a and b. The constant a depends on the turbulence intensity; a precise form is presented later. If second-mode mechanisms are included, the constant b is assigned a value of 0.06, slightly higher than the range of values used in Ref. [3] (0.053 to 0.056). Otherwise, b is set to zero.

Eq. 1 is converted to an evolution equation for an eddy viscosity characteristic of non-turbulent fluctuations by multiplying by $C_\mu \tau_{nt}$ and neglecting derivatives of the surface-dependent quantity τ_{nt}:

$$\begin{aligned} \frac{D\nu_{nt}}{Dt} &= \nu_{nt}\Omega(C_\mu \Omega \tau_{nt} - (a+b)\frac{\nu_{nt}}{\sqrt{2}\nu}) \\ &+ \frac{\partial}{\partial x_j}((\frac{\nu}{3} + 1.8\nu_{nt})\frac{\partial \nu_{nt}}{\partial x_j}) \end{aligned} \tag{9}$$

Eq. 9 is then combined with the Spalart-Allmaras model, with each component weighted by an intermittency function Γ. As Γ approaches zero, the evolution equation for the "non-turbulent" eddy viscosity is recovered, and as Γ approaches one, the standard Spalart-Allmaras model is recovered. Using the notation of Ref. [6], the result is given by the following:

$$\frac{D\tilde{\nu}}{Dt} = (1-\Gamma)\tilde{\nu}\Omega[C_\mu \Omega \tau_{nt} - (a+b)\frac{\tilde{\nu}}{\sqrt{2}\nu}] \tag{10}$$

$$+ C_t \Gamma (1-\Gamma)\tilde{\nu}\Omega$$

$$+ \Gamma[C_{b1}(1-f_{t2})\tilde{\nu}\tilde{\Omega} - (C_{w1} f_w - \frac{C_{b1}}{\kappa^2} f_{t2})(\frac{\tilde{\nu}}{d})^2]$$

$$+ \frac{\Gamma}{\sigma}(\nabla\tilde{\nu})^2 + \nabla \cdot (\frac{1}{\sigma_l}\nu + \frac{1}{\sigma_t}\tilde{\nu})\nabla\tilde{\nu})$$

where

$$\frac{1}{\sigma_l} = \frac{\Gamma}{\sigma} + \frac{1-\Gamma}{3}, \tag{11}$$

$$\frac{1}{\sigma_t} = \frac{\Gamma}{\sigma} + 1.8(1-\Gamma), \tag{12}$$

$\tilde{\nu}$ is the transported quantity (proportional to the eddy viscosity), and d is the distance from the nearest wall. The term $C_t\Gamma(1-\Gamma)\tilde{\nu}\Omega$, which is not present in either Eq. 9 or the Spalart-Allmaras model, affects the behavior of the solution in the transition region $0 < \Gamma < 1$. The chosen value of C_t, 0.35, was determined by numerical optimization, as discussed later. The final step accounts for the viscous sublayer in the fully turbulent region:

$$\nu_t = \tilde{\nu}[1 + \Gamma(f_{v1} - 1)] \tag{13}$$

This step turns off viscous damping in the regions governed by non-turbulent fluctuations. All other constants and functions are as described in Ref. [6], except that the function

$$f_{t2} = C_{t3} \exp(-C_{t4}(\frac{\tilde{\nu}}{\nu})^2) \tag{14}$$

is redefined as

$$f_{t2} = C_{t3} \exp(-C_{t4}(\max[\frac{\sqrt{2}C_\mu \Omega \tau_{nt}}{(a+b)}, \frac{\tilde{\nu}}{\nu}])^2) \tag{15}$$

The additional argument in Eq. 15 is the algebraic solution of Eq. 9, neglecting convective and diffusive terms. This modification helps initiate the turbulent growth process. The "trip" term described in Ref. [6] is not included.

Transition Onset

Transition onset is specified by monitoring the behavior of the quantity

$$R_T = \frac{\tilde{\nu}}{C_\mu \nu} \tag{16}$$

throughout a particular boundary layer profile. When the maximum value of R_T in a profile first exceeds unity ("first" in the sense of a sweep from the stagnation point aft), transition onset is assumed to occur, and the surface distance from that point to the stagnation point is designated as s_t. This step is one of the more geometry-dependent aspects of the model but is somewhat better than other onset indicators, such as the point of minimum heat flux or skin friction, for complex configurations. Ref. [1] shows that, for simpler flowfields, the R_T criterion gives results nearly equivalent to those obtained using a minimum skin friction indicator of transition onset.

Intermittency Definition

The non-turbulent and turbulent components of Eq. 10 are blended through the intermittency function Γ. This is composed of two parts, a surface-distance dependent component $\Gamma_N(s)$ based on the work of Dhawan and Narasimha[7] and a multidimensional component

$\Gamma_b(x, y)$ that serves to restrict the applicable range of the transition model to boundary layers. The particular form is given as follows:

$$\Gamma(x, y) = 1 + \Gamma_b(x, y)(\Gamma_N(s) - 1) \tag{17}$$

The Dhawan-Narasimha expression Γ_N is defined along the surface of the geometry from the stagnation point:

$$\Gamma_N(s) = 1 - \exp(-0.412\xi^2) \tag{18}$$

$$\xi = \max(s - s_t, 0)/\lambda \tag{19}$$

$$Re_\lambda = 9.0 Re_{s_t}^{-0.75} \tag{20}$$

The boundary layer localization function Γ_b is defined as follows:

$$\Gamma_b(x, y) = \tanh(\eta^2), \tag{21}$$

$$\eta = \frac{\max(0, \max(t_1, t_2) - t_\infty)}{t_3 + t_\infty}, \tag{22}$$

$$t_1 = \frac{500\nu}{d^2}, \tag{23}$$

$$t_2 = \frac{\sqrt{(\nu + \nu_t)\Omega}}{C_\mu^{3/2} d}, \tag{24}$$

$$t_3 = \sqrt{C_\mu}\Omega \tag{25}$$

$$t_\infty \approx 1 \times 10^{-7} \frac{U_\infty^2}{\nu_\infty} \tag{26}$$

This expression is similar to that utilized in Menter's hybrid $k-\epsilon$ / $k-\omega$ turbulence model.[8] Γ_b approaches one near solid surfaces and decays sharply to zero as the edge of the boundary layer is approached. For simpler flows, one can also use

$$\Gamma(x, y) = \Gamma_N(s), \tag{27}$$

with equivalent results. The utility of the multidimensional component Γ_b lies in the calculation of transitional flows on complex geometries, where both shear layers (treated as fully turbulent) and boundary layers might be present.

Results

The unified transition / turbulence model described in earlier sections has been implemented into two Navier-Stokes codes: a research version of CFL3D,[9] a cell-centered finite-volume Navier-Stokes solver for 3-D aerodynamic flows, and REACTMB,[10] a cell-vertex finite-volume Navier-Stokes solver for 2-D or axisymmetric reactive flows. The research version of CFL3D[11] utilizes time-derivative preconditioning[12] to enhance solution accuracy and numerical efficiency for low-speed flow calculations. REACTMB also utilizes time-derivative preconditioning. In CFL3D, the unified model is advanced in a weakly-coupled manner, with the solution for eddy viscosity updated after the solution for the main flow variables. In REACTMB, the model is strongly coupled with the main flow equations. Calculations that account for second-mode disturbances will be specifically noted in the discussion. A baseline convergence criterion of a seven-decade reduction in the residual norm was used for REACTMB, with the cases used in the grid convergence studies converged to even tighter tolerances. Convergence for CFL3D was assessed by monitoring lift and drag coefficients and predicted transition points, as residual norms tended to oscillate after a period of rapid decrease.

Validation of the new approach is accomplished through simulations of several flows successfully computed by the original Warren-Hassan transition / turbulence model. Simulations of the flat-plate experiments of Schubauer and Klebanoff[13] and Schubauer and Skramstad[14] are used to determine the functional dependence of the model constant a on the free-stream turbulence intensity Tu, expressed as a percentage value. The results, obtained by correlating the predicted transition onset locations with experimental data, yield the following dependence:

$$a \doteq 0.009863 - 0.001801(Tu) + 0.05050(Tu)^2 \tag{28}$$

It should be noted that the calibration is also sensitive to the freestream value of the transported quantity $\tilde{\nu}$. This is chosen as $0.0001\nu_\infty$ for all calculations presented herein. The effect of the constant C_t in Eq. 10 on the skin friction predictions for the Schubauer-Klebanoff experiment ($Tu = 0.03$) is shown in Figure 1 (CFL3D implementation). All choices predict the correct onset location based on the $R_T = 1$ criterion, as per the calibration, but the shape of the skin friction distribution is best predicted by the optimized value of $C_t = 0.35$. This value is maintained for all subsequent calculations.

In addition to the 65x97 grid, medium (129x193) and fine (257x385) mesh levels are used to assess the accuracy of the CFL3D solutions. In addition, the Richardson Extrapolation procedure[15] is used to obtain more accurate skin friction profiles:

$$\phi_{RE} = \phi_1 + (\phi_1 - \phi_2)/3 \tag{29}$$

where 1 and 2 denote the fine and medium grid solutions, respectively, and ϕ represents the skin friction. Richardson Extrapolation assumes that the spatial accuracy is second order and that the solutions are in the asymptotic grid convergence regime. Figure 2 presents computed skin friction profiles for the three grid levels along with the Richardson Extrapolation results. Only the results in the transitional region appear to show dependence on the mesh size. The assumptions that the solutions are second order accurate and in the asymptotic grid convergence regime can be assessed by examining the percent error in the solution values relative to the Richardson Extrapolation value:

$$\% \text{ Error of Mesh k} = \frac{(\phi_k - \phi_{RE})}{\phi_{RE}} \times 100 \tag{30}$$

In order for these assumptions to hold, it is necessary (although not sufficient) that the percent error obey the relationship

$$\% \text{ Error of Mesh 1} = \frac{(\%\text{Error of Mesh 2})}{4} = \frac{(\%\text{Error of Mesh 3})}{16} \tag{31}$$

where the left equality in Eq. 31 is identically true when Eq. 29 is used. The normalized errors from Eq. 30 are presented in Figure 3 for the CFL3D solutions of the Schubauer-Klebanoff flat plate case. The skin friction in the laminar and turbulent regions does appear to be within the second order asymptotic grid convergence regime. The fine grid errors in this region are below 1%, while the solutions in the transitional region do not appear to be fully grid converged. This latter result is not surprising since no attempt has been made to provide *a priori* clustering in this region.

Figure 4 illustrates the effect of grid refinement on the skin friction prediction for the $Tu = 0.03$ case, REACTMB implementation. Again, solutions are presented on the three mesh levels along with the Richardson Extrapolation results. Grid sensitivity is seen in both the transitional and turbulent regions of the flow. Figure 4 also shows that the predicted transition location and the extent of the transition region display some sensitivity to the mesh size. The normalized errors from Eq. 31 are presented in Figure 5 and show that the fine grid solution is accurate to within 1% in the laminar region and approximately 3% in the turbulent region. Although these errors are small, the fact that the normalized errors do not satisfy Eq. 31 indicates that the assumptions required for the application of Richardson Extrapolation are not fully valid. Thus, the error estimates presented in Fig. 5 may not be accurate. It is expected that these errors could be further reduced with additional grid refinement and/or grid adaptation. Finally, Figure 6 compares fine grid solutions from the two codes with experimental data for the $Tu = 0.03$ case. Even with significant grid refinement, the solutions do display some code- and implementation-dependent differences.

The second case considered involves the database of Mateer, et al.,[16] which contains skin friction measurements over a supercritical airfoil for a freestream Mach number of 0.2 and a range of Reynolds numbers and angles of attack. The percentage turbulence intensity is $Tu = 0.5$, higher than the highest value found in the Schubauer-Skramstad database ($Tu = 0.34$). For this level of intensity, the model operates slightly outside its limits of calibration. Figure 7 presents skin friction distributions for a Reynolds number of 2×10^6 (based on a 0.2 m chord) and an angle-of-attack of -0.5 degrees. The CFL3D implementation is used for this case. Calculations from a boundary-layer integral / e^n analysis yielded transition predictions well aft of the experimental results for both surfaces.[16] The unified one-equation model predicts transition accurately on the lower surface but aft of the experimental location on the upper surface. These results are in accord with those presented earlier for the Warren-Hassan implementation.[1] Figure 8 compares predictions and experimental results for a higher Reynolds number of 6×10^6. Good agreement with the upper-surface transition location is indicated, but the model underpredicts the extent of laminar flow on the lower surface. It is of note that the predicted transition locations for both cases are nearly equal for the upper and lower surfaces, a trait also shared by the Warren-Hassan implementation. This may indicate the need for the explicit inclusion of surface pressure gradient effects into the correlation for τ_{nt} to render it more valid for curved surfaces.

The third test case involves Mach 0.2, $\alpha = 19°$ flow about a three-element airfoil in landing configuration.[17, 18, 19] This configuration has been the subject of a detailed investigation using the original Warren-Hassan transition / turbulence model.[4] Results using the baseline Spalart-Allmaras model with either user-specified transition points or "natural" transition have also been reported.[18] Figures 9, 10, and 11 compare velocity magnitude profiles at the $x/c = 0.1075$, $x/c = 0.45$, and $x/c = 0.8982$ locations (relative to the stowed chord length) with experimental data from Chin, et al.[17] Profiles were measured only along the upper surfaces of the airfoils and are plotted versus normal distance from the surface. These calculations were run using the modified CFL3D code, assuming a free-stream turbulence intensity of $Tu = 0.05$. The figures include results from the unified model implemented using the one-dimensional intermittency function $\Gamma = \Gamma_N(s)$ (Eq. 27), results from the unified model implemented using the two-dimensional intermittency function $\Gamma = \Gamma(x, y)$ (Eq. 17), and results from a fully turbulent implementation. In comparison with the fully turbulent model, the unified model provides better agreement with experimental data for the stations nearer the leading edge but provides poorer agreement further downstream. Close agreement between predictions using the one-dimensional intermittency function and those using the two-dimensional intermittency function is evidenced for all stations. The success of the one-dimensional intermittency function in this case may be fortuitous, as the grid blocking arrangement is such that the presence of transitional regions extending away from the element surfaces does not interfere significantly with turbulent wake development. In accord with experimental results,[19] the unified model predicts a nearly laminar slat cove and a nearly laminar undersurface of the flap. The model does, however, predict transition on the lower surface of the main element as occurring at roughly the quarter-chord point. Experimental data suggests that transition on this surface is delayed until the flap cove. Contour plots of $\Gamma(x, y)$ are shown in Figure 12 for the slat - main-element juncture. As indicated, the transition model with $\Gamma = \Gamma(x, y)$ is localized to initially laminar boundary layers near the surface of each element. Shear layers are treated in a fully turbulent fashion.

The fourth test case involves transitional, Mach 3.5 flow over a 5 degree half-angle cone and corresponds to a set of experiments conducted by Chen, et al.[20] in the NASA Langley Mach 3.5 Pilot Low Disturbance Wind Tunnel. This case has also been studied by Singer, et al.[21], Warren, et al.[22], and McDaniel, et al.[3], with the two latter efforts using variants of the Warren-Hassan transition model. Figure 13 presents wall recovery factor as a function of surface distance along the cone. The wall recovery factor is defined by the relation

$$r = \frac{T_{aw} - T_e}{T_o - T_e}$$

where

$$T_o = T_e(1 + \frac{\gamma - 1}{2} M_e^2)$$

and T_{aw} and T_e are determined from the computed solution at the wall and at the edge of the boundary layer. The calculations assume that only first-mode mechanisms are important and assume a turbulent Prandtl number of 0.88 and a turbulence intensity of 0.05. Furthermore, the calculations were performed using the REACTMB implementation. As noted in Ref. [22], recovery factor predictions for this flow are very sensitive to the assumed value of the turbulent Prandtl number, with the commonly-used value of 0.9 resulting in a sizeable overprediction in the transitional and turbulent regions. Ref. [22] also shows that agreement with experimental data can be substantially improved by including a flow-dependent turbulent Prandtl number; such techniques have yet to be implemented in the present work. The current results indicate that the unified one-equation model accurately predicts the onset of transition for each of the Reynolds numbers considered. The model does overestimate the peak in recovery factor near the end of the transition region and slightly overpredicts the recovery factor in the fully-turbulent region. The former effect may indicate the need for improved modeling of the transition-region term

$$C_t \Gamma (1 - \Gamma) \tilde{\nu} \Omega$$

in Eq. 10 for high-speed flows.

Three grid levels are used to assess the accuracy of the calculations for the Re/m = 5.89×10^7 case. Figure 14 shows the recovery factor profiles for the three grid levels along with the Richardson Extrapolation results using Eq. 29. The most noteworthy effects of increasing mesh refinement are a decrease in the distance required to establish an equilibrium laminar boundary layer, a lowering of the recovery factor in the fully turbulent region, and a slight shift in the transition onset location downstream. The error in recovery factor relative to the more accurate extrapolated values are given in Figure 15, where the errors have been normalized according to Eq. 31. The fine grid errors are well below 0.1% in the laminar and turbulent regions. The collocation of the normalized errors indicates the locations where the solution is likely in the asymptotic grid convergence regime. Larger errors are seen at the stagnation point singularity and in the transition region due to the large gradients. Additional grid clustering could be employed to reduce the magnitude of the error in these regions.

The final test case considered in this article involves Mach 5.91 flow over an 18 inch flared cone and corresponds to the experiments of Blanchard and Selby[23], conducted in the NASA Langley Mach 6 quiet tunnel. The geometry consists of a straight 5 degree half angle cone for the first 10 inches, followed by a flared portion with a radius of curvature of 91.94 inches. The flared portion was designed to induce a mild adverse pressure gradient, hastening the growth of second-mode disturbances deemed important for natural transition in hypersonic flows. A 241x221 mesh, clustered to the cone apex and to the wall, is used. This case was also studied in Ref. [3] using the Warren-Hassan transition / turbulence model. Figure 16 compares wall temperature predictions with experimental data. Both second and first-mode contributions are included in the transition model. The neglect of second-mode contributions resulted in laminarization, while second-mode contributions alone resulted in premature transition on the straight cone section. In the laminar part of the flow, the calculations underpredict the wall temperature, with an average percent error of around 2 %. In the transitional region, the calculated temperatures are again below the experimental values, with an average percent error of around 9%. Surface values of the intermittency function are around 0.77 near the end of the flare, indicating that the calculation never attains a fully turbulent state. Calculations performed on a finer grid of 481x441 nodes (not shown) failed to provide any substantial improvement over these results. This level of disagreement was also seen in the predictions of Ref. [3], but as noted in that reference, there are inconsistencies in the presentation of the experimental results that defy a simple explanation. Nevertheless, the unified model provides reasonable qualitative agreement with the experimental data, with predicted transition onset delayed until the flared portion of the cone (X $\approx$ 14 inches).

Conclusions

A unified, one-equation "eddy viscosity - transport" model for transitional and turbulent flows has been developed. The model combines an evolution equation for non-turbulent fluctuation growth developed from the work of Warren and Hassan with the standard Spalart-Allmaras turbulence model. Blending of the two equations is accomplished through a multidimensional intermittency function. The current formulation is calibrated for transition driven by the growth of first- and second-mode instabilities and predicts both the onset and extent of the transition region. The model has been applied with reasonable success to low-speed transitional flows over a flat plate, a supercritical airfoil, and a multi-element airfoil in landing configuration and to high-speed flows over cone and flared-cone configurations. The predictions are very similar to those obtained earlier using the $k - \zeta$ turbulence model, indicating that the performance of the Warren-Hassan model in predicting transitional flows is relatively independent of the turbulence model used. Grid refinement studies for selected cases indicate that the prediction of transition onset is relatively insensitive to the grid spacing for the finer meshes but that grid refinement or grid adaptation may be required to obtain grid independence in the prediction of the extent of the transition region.

Acknowledgements

This research is sponsored by Sandia National Laboratories under Contract BF-856. Cray T-90 computer time is provided by a grant from the North Carolina Supercomputing Center. The authors would like to thank Melissa Manning of North Carolina State University for providing the mesh used in the flared-cone calculations.

References

[1] Warren, E.S. and Hassan, H.A. "Transition Closure Model for Predicting Transition Onset," *Journal of Aircraft*,Vol. 35, No. 5, 1998, pp. 769-775.

[2] Warren, E.S., and Hassan, H.A. "An Alternative to the e^n Method for Determining Onset of Transition," AIAA Paper 97-0825, Jan., 1995.

[3] McDaniel, R., Nance, R.P., Hassan, H.A. "Transition Onset Prediction for High Speed Flow," AIAA Paper 99-3792, June, 1999.

[4] Czerwiec, R., Edwards, J.R., Rumsey, C.L., Bertelrud, A., and Hassan, H.A. "Study of High-Lift Configurations Using $k-\zeta$ Transition / Turbulence Model," AIAA Paper 99-3186, June, 1999. To appear in *Journal of Aircraft.*

[5] Robinson, D.F. and Hassan, H.A. "Further Development of the $k-\zeta$ (Enstrophy) Turbulence Closure Model," *AIAA Journal,* Vol. 36, No. 10, 1998, pp. 1825-1833.

[6] Spalart, P.R. and Allmaras, S.R. "A One-Equation Turbulence Model for Aerodynamic Flows," *La Recherche Aerospatiale*, Vol 1., 1994, pp. 5-21.

[7] Dhawan, S. and Narasimha, R. "Some Properties of Boundary Layer Flow During Transition from Laminar to Turbulent Motion," *Journal of Fluid Mechanics,* Vol. 3, No. 4, pp. 418-436, 1958.

[8] Menter, F.R. "Two-Equation Eddy Viscosity Turbulence Models for Engineering Applications," *AIAA Journal*, Vol. 32, No. 8, 1994, pp. 1598-1605.

[9] Thomas, J.L., Taylor, S.L., and Anderson, W.K. "Navier-Stokes Computations of Vortical Flows over Low Aspect Ratio Wings," AIAA Paper 87-0207, 1987.

[10] McDaniel, K.S., and Edwards, J.R. "Simulation of Thermal Choking in a Model Scramjet Combustor," AIAA Paper 99-3411, June, 1999.

[11] Edwards, J.R. and Thomas, J.L. "Development of $\mathcal{O}(Nm^2)$ Preconditioned Multigrid Solvers for the Euler and Navier-Stokes Equations," *AIAA Journal*, Vol. 34, No. 4, 2000, pp. 717-720.

[12] Weiss, J.M., and Smith, W.A. "Preconditioning Applied to Variable and Constant Density Time-Accurate Flows on Unstructured Meshes," AIAA Paper 94-2209, June,1994.

[13] Schubauer, G.B. and Klebanoff, P.S. "Contributions on the Mechanism of Boundary Layer Transition," NACA Report 1289, 1956.

[14] Schubauer, G.B. and Skramstad, H.K. "Laminar Boundary Layer Oscillation on a Flat Plate," NACA Report 909, 1948.

[15] Roache, P. J., "Ch. 5: Systematic Grid Convergence Studies and the Grid Convergence Index (GCI)," Verification and Validation in Computational Science and Engineering, Hermosa Publishers, New Mexico, 1998, p. 109.

[16] Mateer, G.G., Monson, D.J., and Menter, F.R. "Skin Friction Measurements and Calculations on a Lifting Airfoil," *AIAA Journal*, Vol. 34, No. 2, 1996, pp. 231-236.

[17] Chin, V.D., Peters, D.W., Spaid, F.W., and McGhee, R.J. "Flowfield Measurements About a Multi-Element Airfoil at High Reynolds Numbers," AIAA Paper 93-3137, July, 1993.

[18] Rumsey, C.L., Gatski, T.B., Ying, S.Y., and Bertelrud, A. "Prediction of High-Lift Flows Using Turbulent Closure Models," *AIAA Journal*, Vol. 36, No. 5, 1998, pp. 765-774.

[19] Bertelrud, A., "Transition on a Three-Element High-Lift Configuration at High Reynolds Numbers," AIAA Paper 98-0703, Jan. 1998.

[20] Chen, F.J., Malik, M.R., and Beckwith, I.E., "Boundary Layer Transition on a Cone and Flat Plate at Mach 3.5," *AIAA Journal*,Vol. 27, No. 6, 1989, pp. 687-693.

[21] Singer, B.A., Dinavahi, S.P.G., and Iyer, V., "Testing of Transition Region Models: Test Cases and Data," NASA CR 4371, May, 1991.

[22] Warren, E.S., Harris, J.E., and Hassan, H.A. "Transition Model for High-Speed Flow," *AIAA Journal*, Vol. 33, No. 8, 1995, pp. 1391-1397.

[23] Blanchard, A.E., and Selby, G.V. "An Experimental Investigation of Wall-Cooling Effects on Hypersonic Boundary Layer Stability in a Quiet Wind Tunnel," NASA CR-198287, Feb., 1996.

Figure Captions

Figure 1: Effect of C_t on skin friction distribution (Schubauer-Klebanoff experiment; 65x97 mesh; CFL3D implementation)

Figure 2: Skin friction distributions for the Schubauer-Klebanoff flat plate along with Richardson Extrapolation results (CFL3D implementation)

Figure 3: Normalized error in skin friction on the three mesh levels for the Schubauer-Klebanoff flat plate (CFL3D implementation).

Figure 4: Skin friction distributions for the Schubauer-Klebanoff flat plate along with Richardson Extrapolation results (REACTMB implementation).

Figure 5: Normalized error in skin friction on the three mesh levels for the Schubauer-Klebanoff flat plate (REACTMB implementation).

Figure 6: Fine-grid skin friction predictions versus experimental data (Schubauer-Klebanoff experiment)

Figure 7: Skin friction distributions (Mateer supercritical airfoil, $\mathrm{Re}_c = 2 \times 10^6$, 321x91 mesh)

Figure 8: Skin friction distributions (Mateer supercritical airfoil, $\mathrm{Re}_c = 6 \times 10^6$, 321x91 mesh)

Figure 9: Velocity profiles (x/c = 0.1075 station, $\alpha = 19°$)

Figure 10: Velocity profiles (x/c = 0.45 station, $\alpha = 19°$)

Figure 11: Velocity profiles (x/c = 0.8982 station, $\alpha = 19°$)

Figure 12: Intermittency contours (localized to thin, nearly laminar boundary layers)

Figure 13: Measured and computed recovery factors (M = 2.5, Re/m = 3.85×10^7, 5.89×10^7, 7.8×10^7, $Pr_t = 0.88$)

Figure 14: Recovery factor distributions for the Mach 3.5 cone along with Richardson Extrapolation results

Figure 15: Normalized error in recovery factor on the three mesh levels for the Mach 3.5 cone

Figure 16: Measured and computed adiabatic wall temperatures (M = 5.91, Re/m = 9.348×10^6, $T_\infty = 56.2$ K, 241x225 mesh)

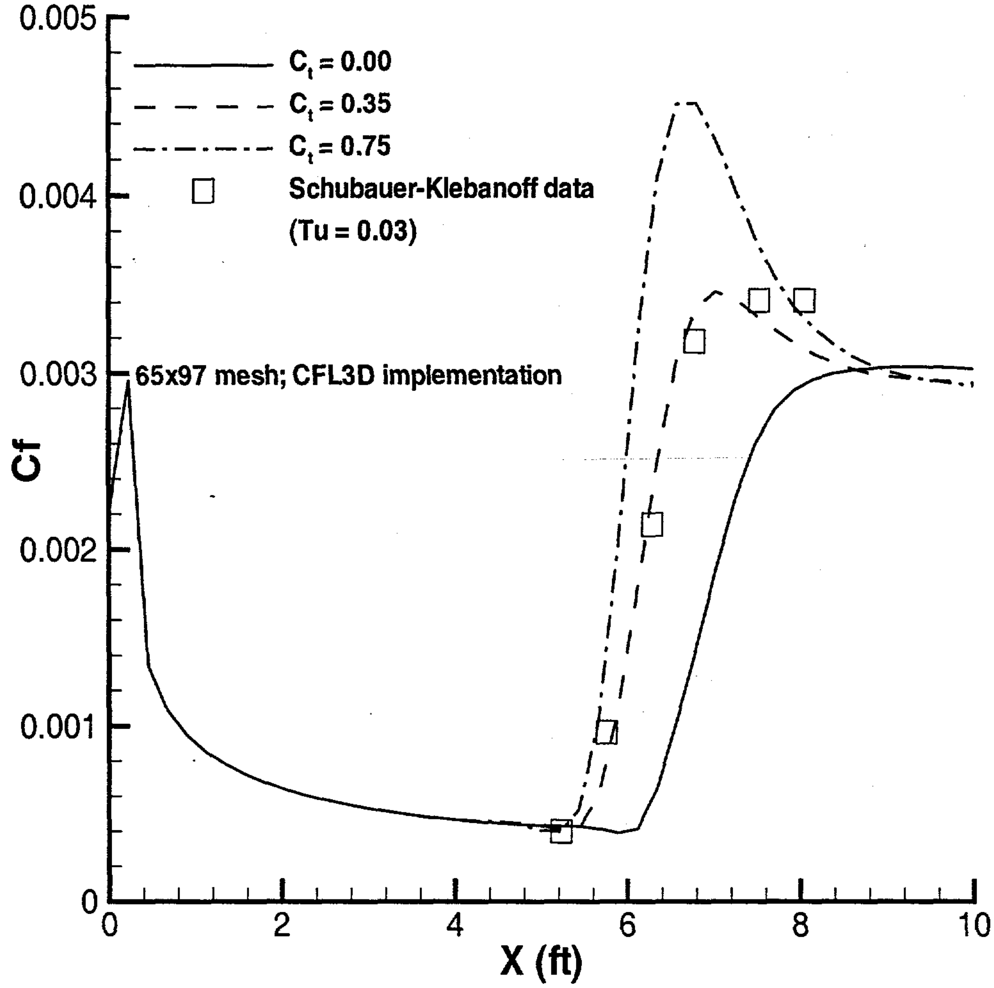

0.005
0.004
0.003
0.002
0.001
0
Cf
$C_t = 0.00$
$C_t = 0.35$
$C_t = 0.75$
Schubauer-Klebanoff data
(Tu = 0.03)
65x97 mesh; CFL3D implementation
0
2
4
6
8
10
X (ft)

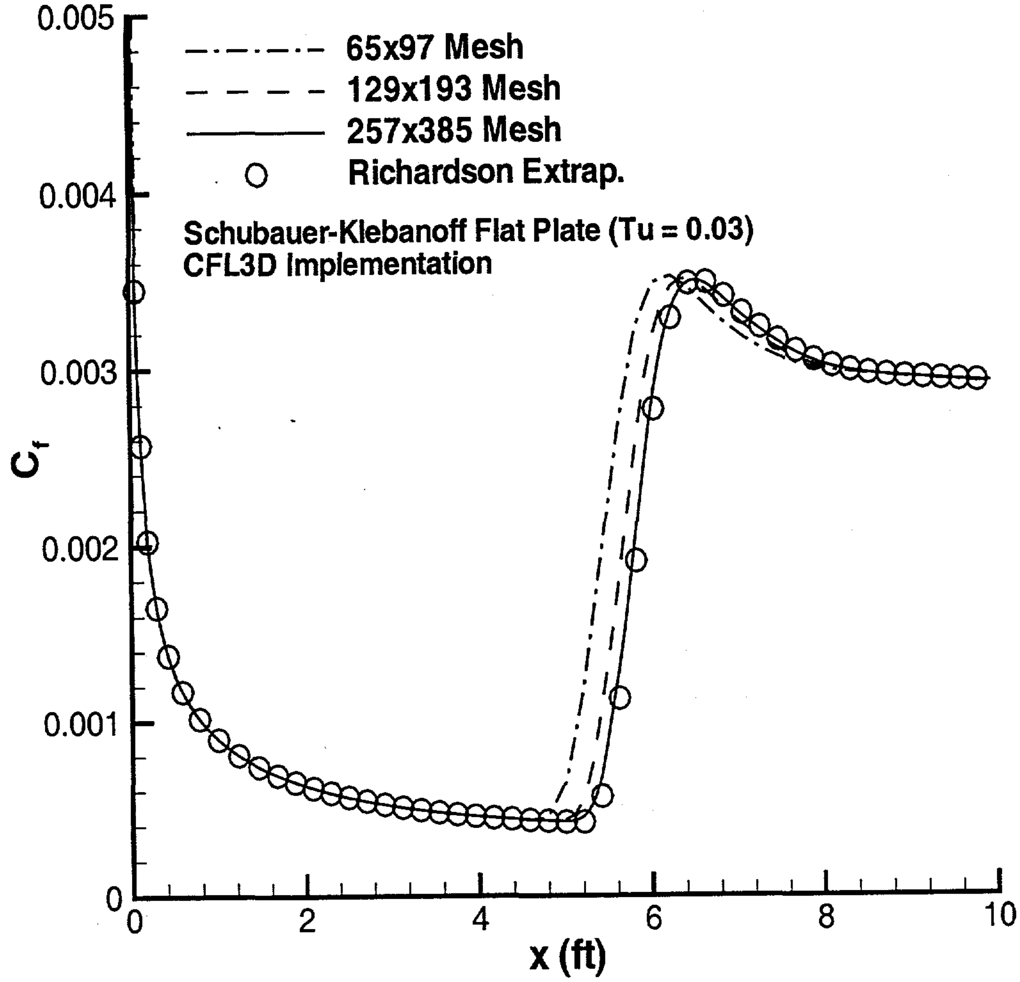

0.005
0.004
0.003
0.002
0.001
0
C_f
0
2
4
6
8
10
x (ft)
65x97 Mesh
129x193 Mesh
257x385 Mesh
Richardson Extrap.
Schubauer-Klebanoff Flat Plate (Tu = 0.03)
CFL3D Implementation

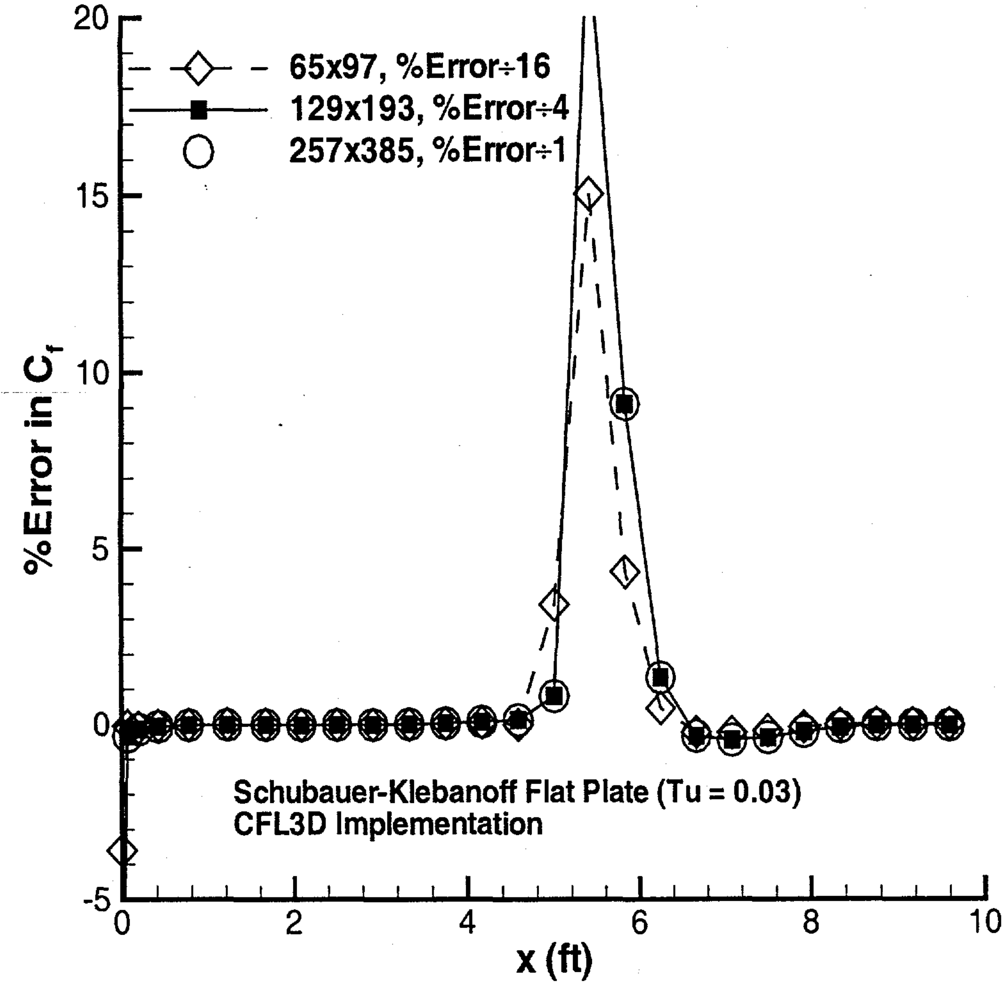

65x97, %Error÷16
129x193, %Error÷4
257x385, %Error÷1
%Error in C_f
x (ft)
Schubauer-Klebanoff Flat Plate (Tu = 0.03)
CFL3D Implementation
20
15
10
5
0
-5
0
2
4
6
8
10

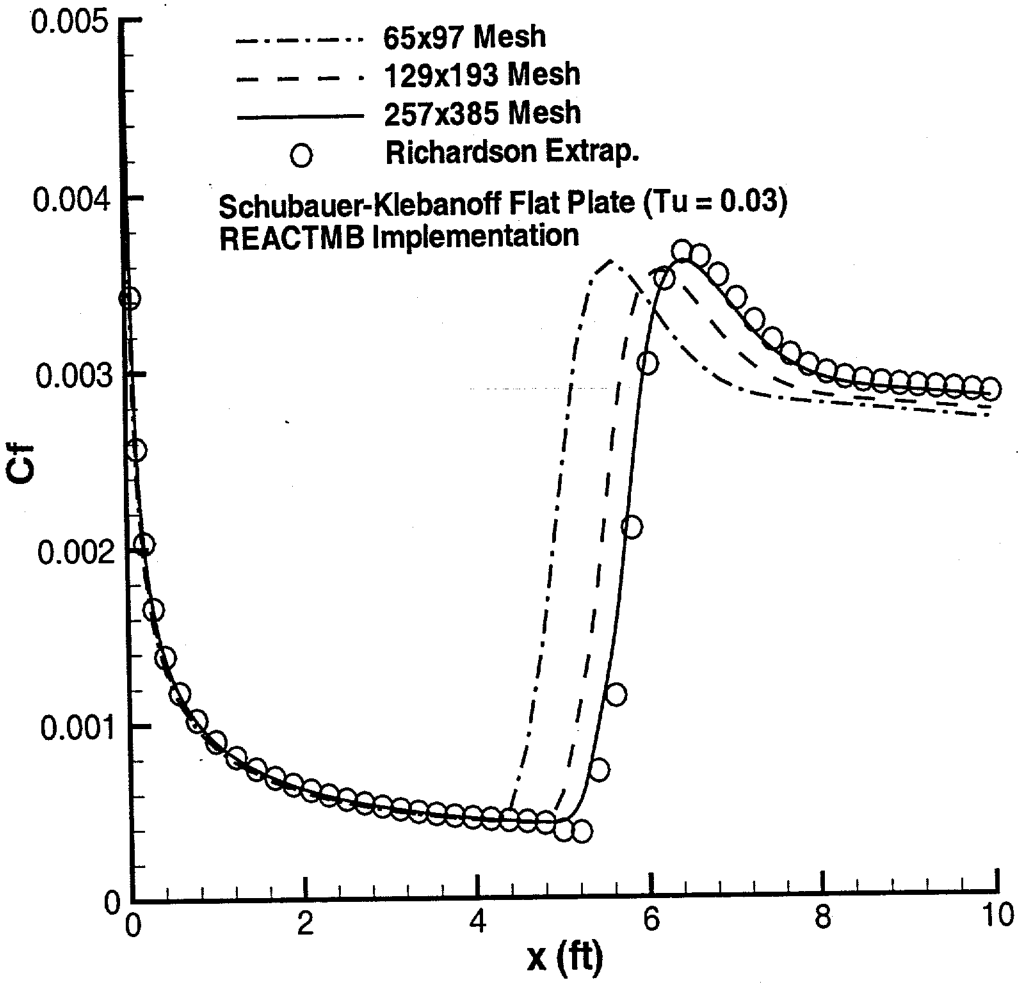
65x97 Mesh
129x193 Mesh
257x385 Mesh
Richardson Extrap.
Schubauer-Klebanoff Flat Plate (Tu = 0.03)
REACTMB Implementation
Cf
x (ft)
0.005
0.004
0.003
0.002
0.001
0
0
2
4
6
8
10

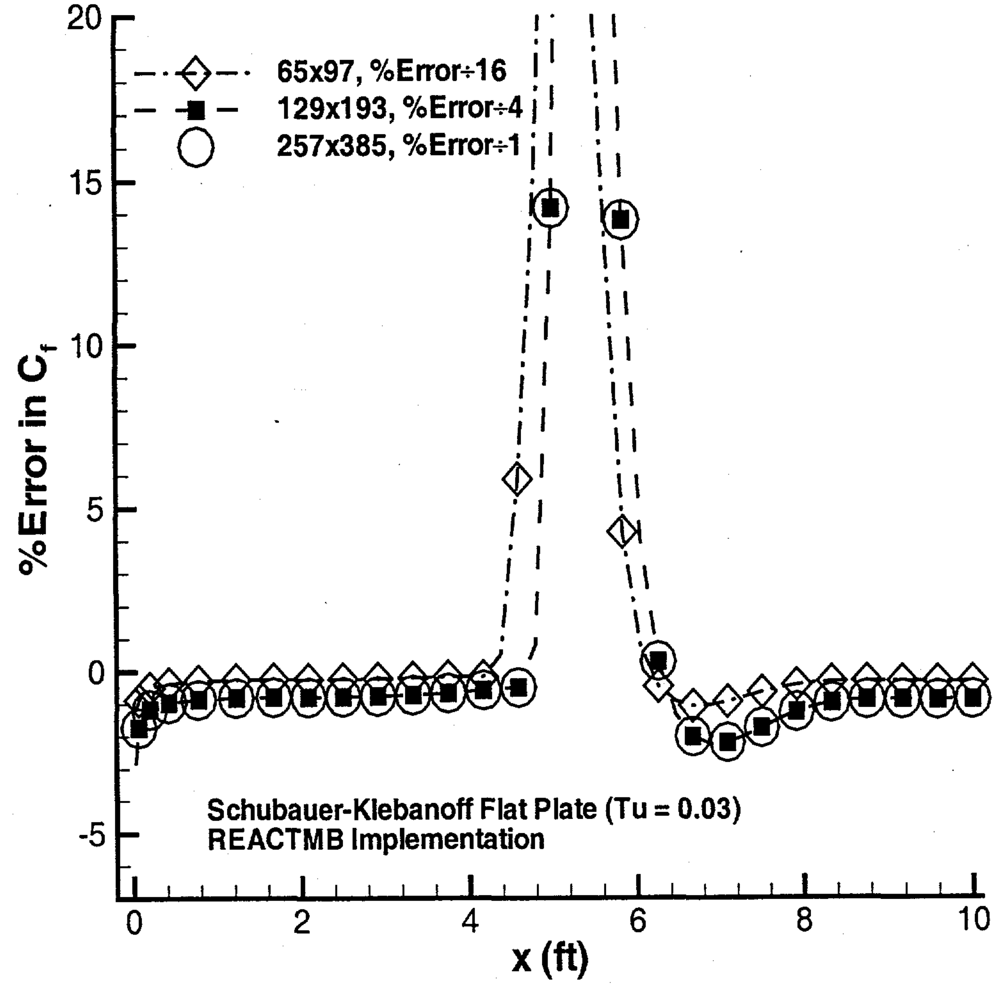
65x97, %Error÷16
129x193, %Error÷4
257x385, %Error÷1
%Error in C_f
20
15
10
5
0
-5
0
2
4
6
8
10
x (ft)
Schubauer-Klebanoff Flat Plate (Tu = 0.03)
REACTMB Implementation

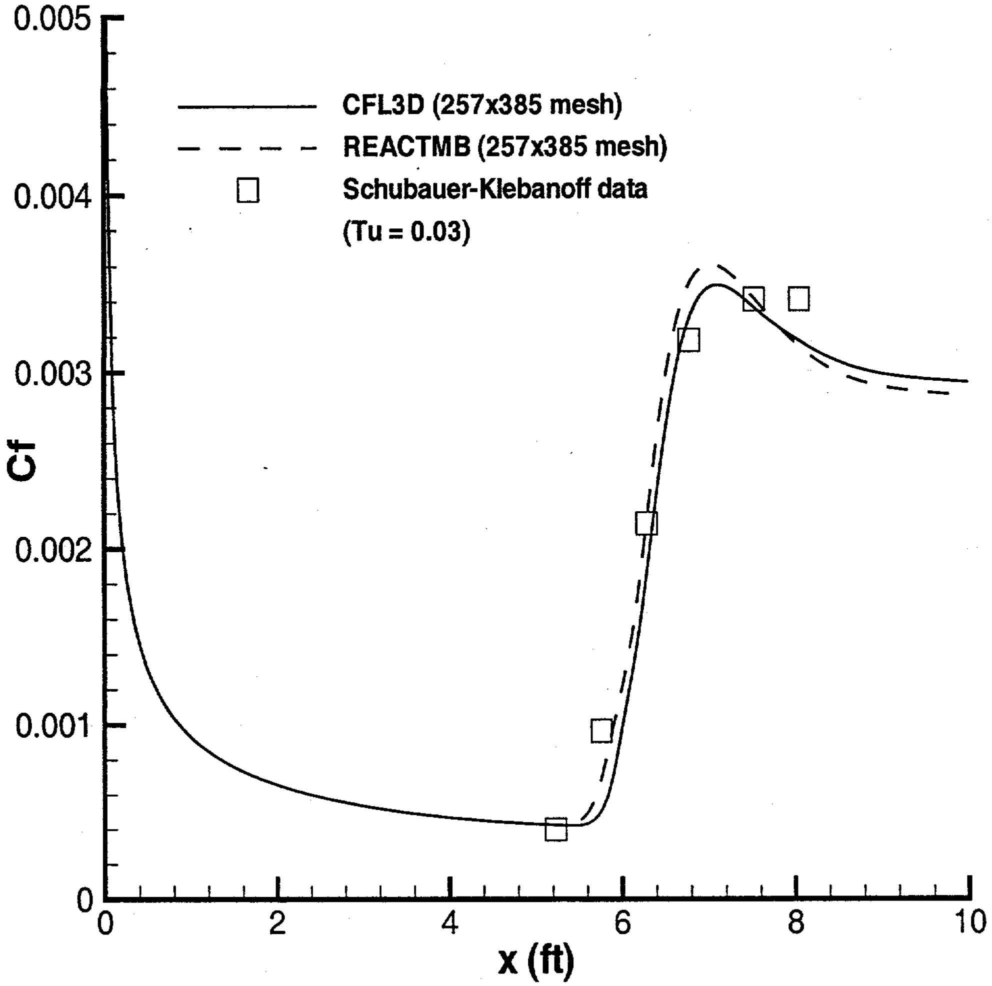

0.005
0.004
0.003
0.002
0.001
0
Cf
CFL3D (257x385 mesh)
REACTMB (257x385 mesh)
Schubauer-Klebanoff data
(Tu = 0.03)
0
2
4
6
8
10
x (ft)

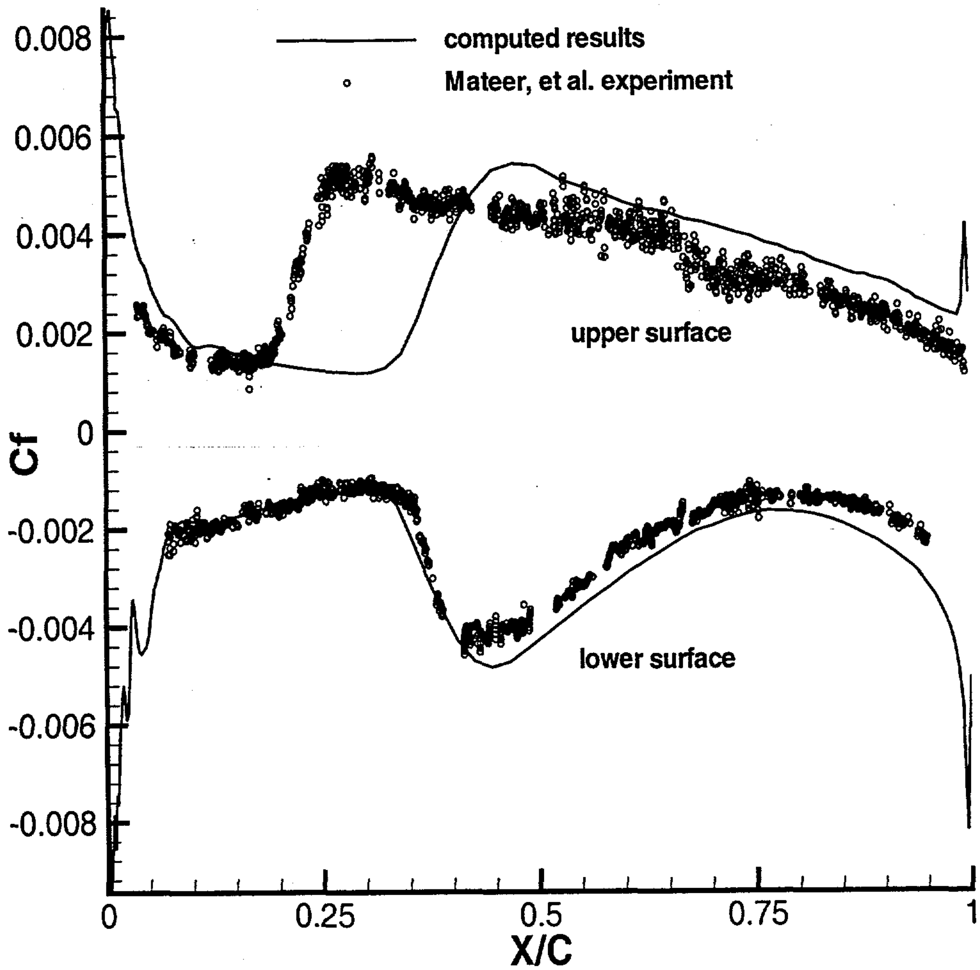
computed results
Mateer, et al. experiment
upper surface
lower surface
Cf
X/C
0.008
0.006
0.004
0.002
0
-0.002
-0.004
-0.006
-0.008
0
0.25
0.5
0.75
1

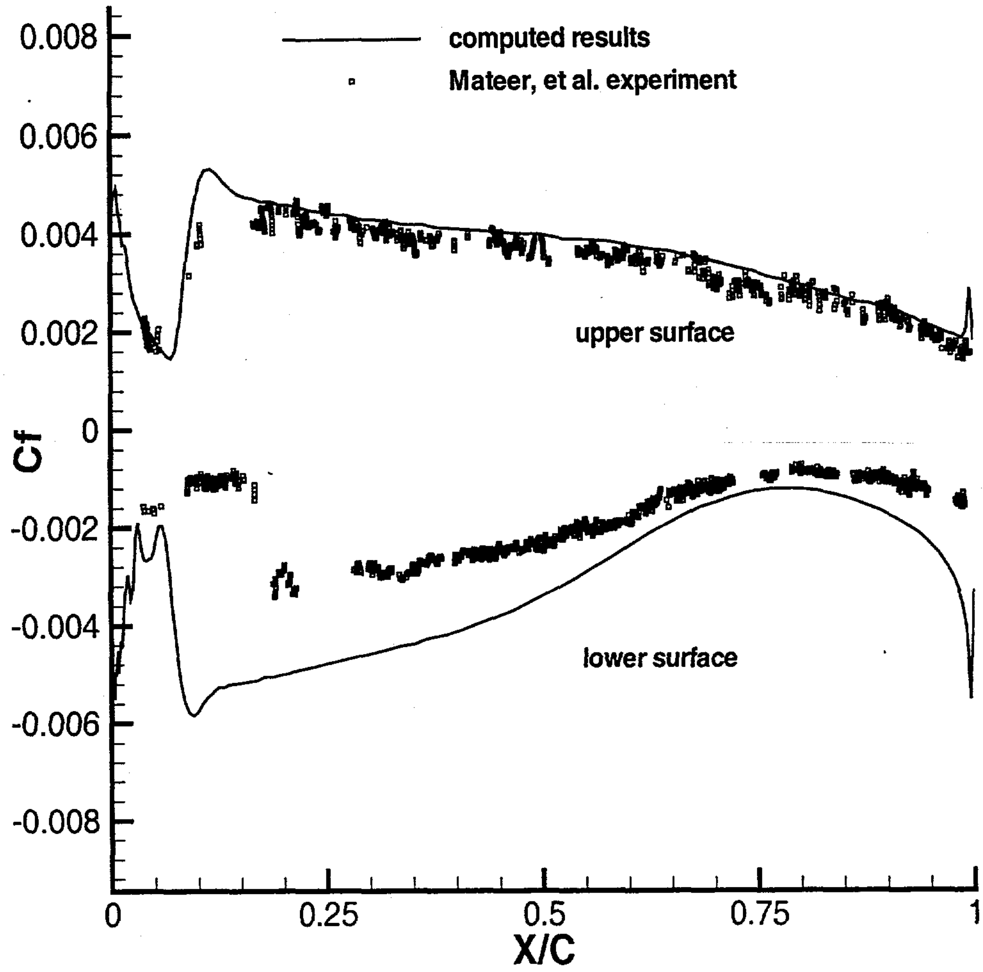
computed results
Mateer, et al. experiment
upper surface
lower surface
Cf
X/C
0.008
0.006
0.004
0.002
0
-0.002
-0.004
-0.006
-0.008
0
0.25
0.5
0.75
1

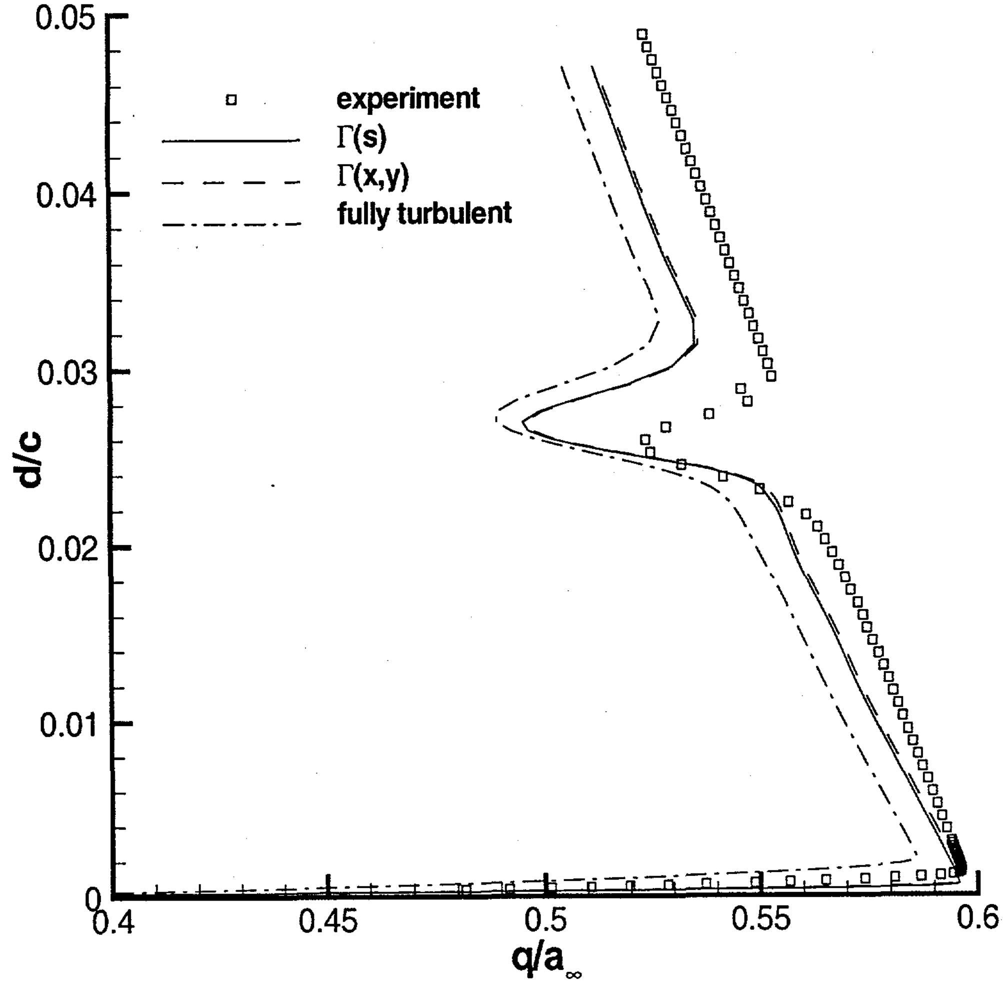
0.05
0.04
0.03
0.02
0.01
0
d/c
experiment
Γ(s)
Γ(x,y)
fully turbulent
0.4
0.45
0.5
0.55
0.6
q/a∞

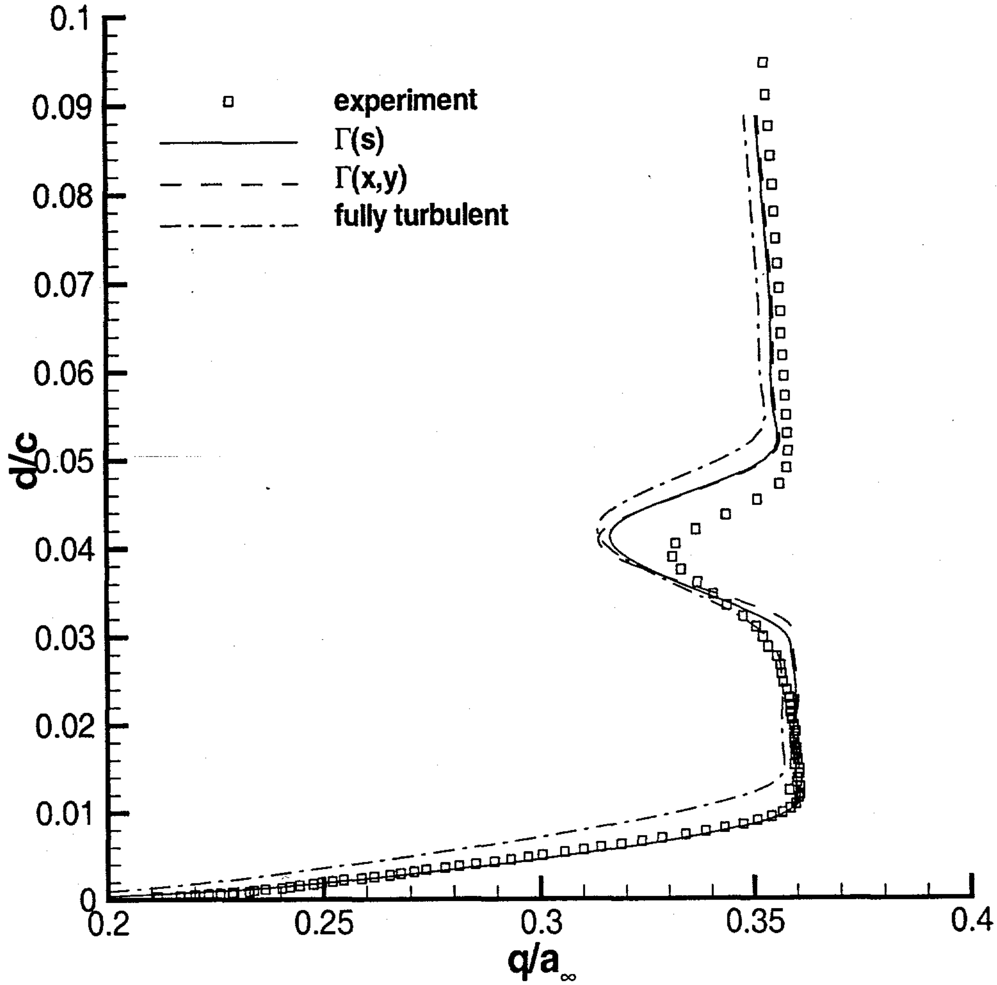

0.1
0.09
0.08
0.07
0.06
0.05
0.04
0.03
0.02
0.01
0
d/c
experiment
Γ(s)
Γ(x,y)
fully turbulent
0.2
0.25
0.3
0.35
0.4
q/a∞

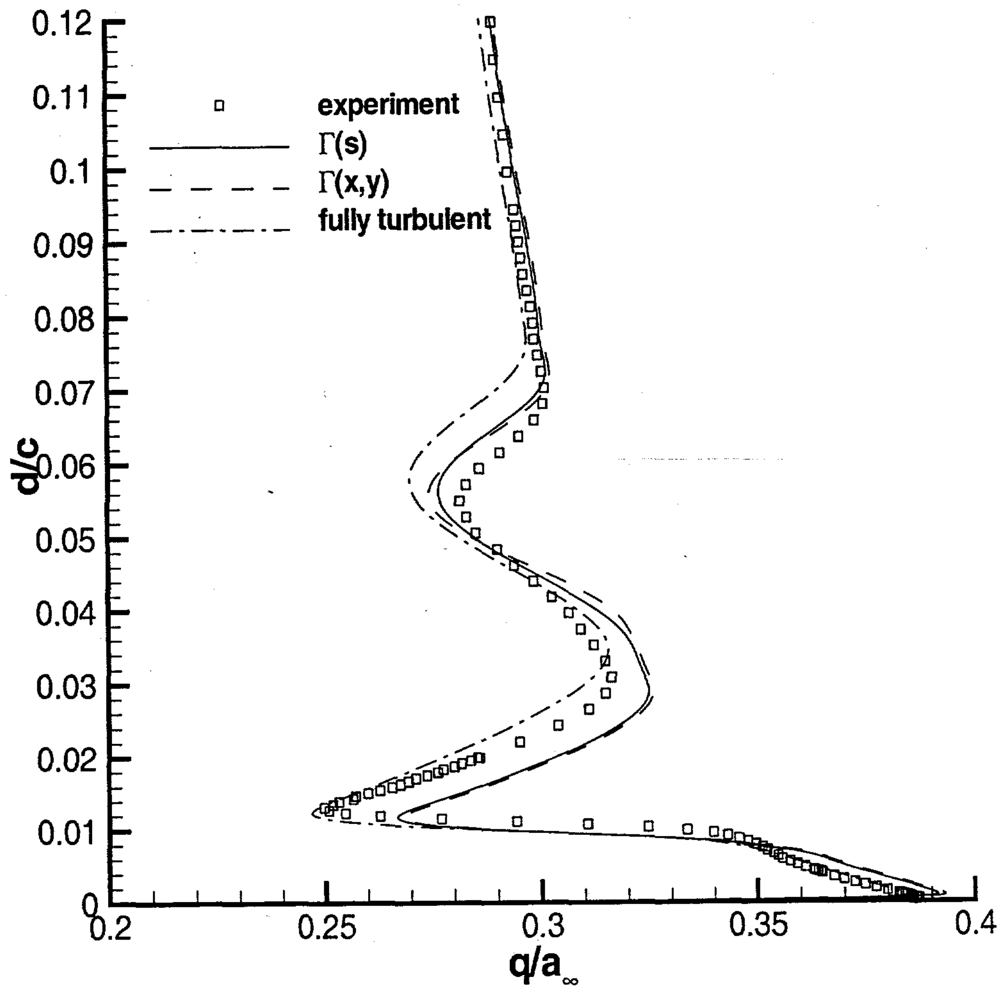
0.12
0.11
0.1
0.09
0.08
0.07
0.06
0.05
0.04
0.03
0.02
0.01
0
d/c
experiment
Γ(s)
Γ(x,y)
fully turbulent
0.2
0.25
0.3
0.35
0.4
q/a∞

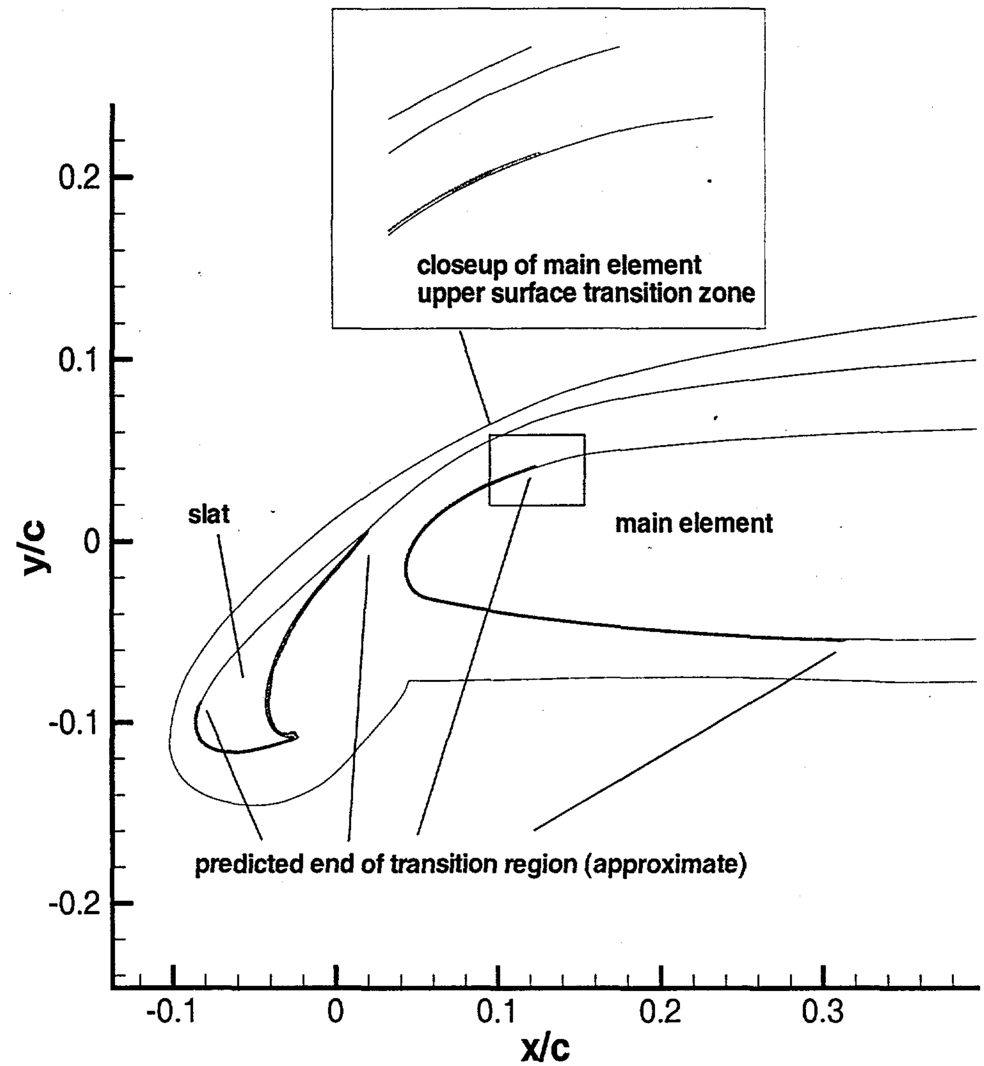
closeup of main element
upper surface transition zone
0.2
0.1
0
-0.1
-0.2
y/c
slat
main element
predicted end of transition region (approximate)
-0.1
0
0.1
0.2
0.3
x/c

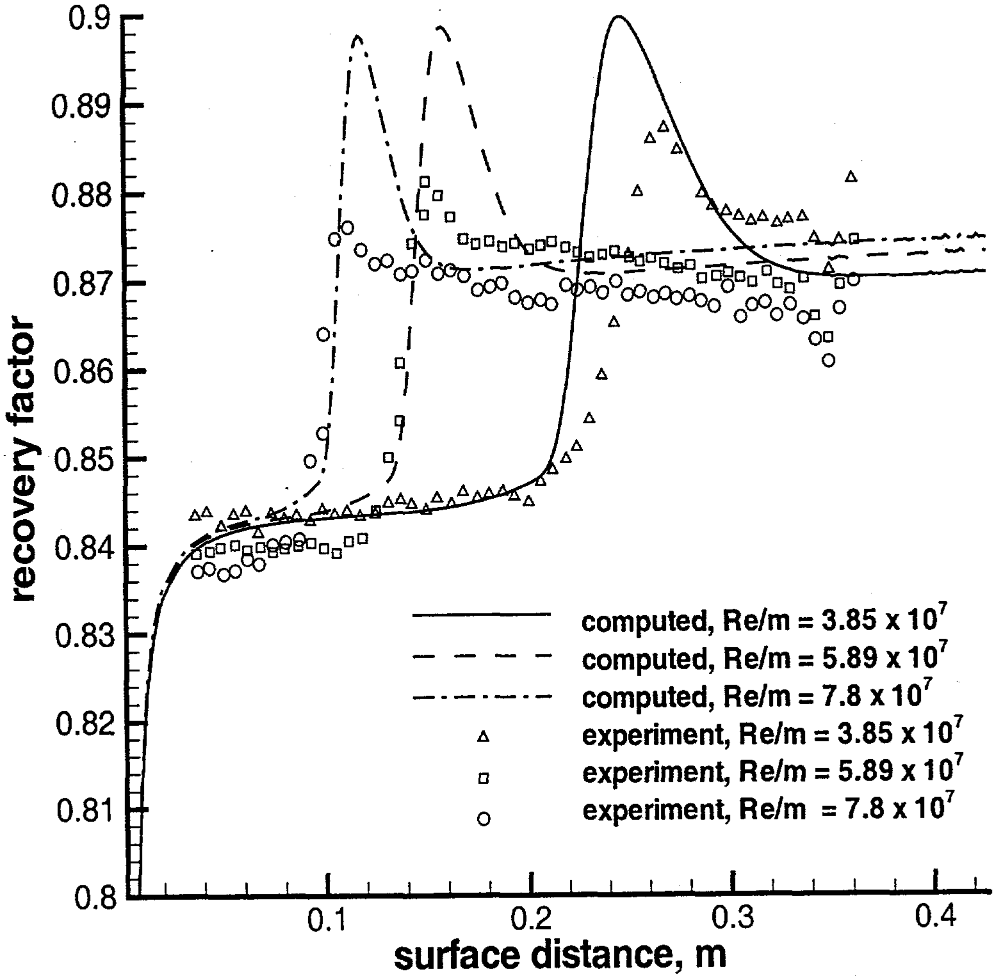
0.9
0.89
0.88
0.87
0.86
0.85
0.84
0.83
0.82
0.81
0.8
recovery factor
0.1
0.2
0.3
0.4
surface distance, m
computed, Re/m = 3.85 x 10^7
computed, Re/m = 5.89 x 10^7
computed, Re/m = 7.8 x 10^7
experiment, Re/m = 3.85 x 10^7
experiment, Re/m = 5.89 x 10^7
experiment, Re/m = 7.8 x 10^7

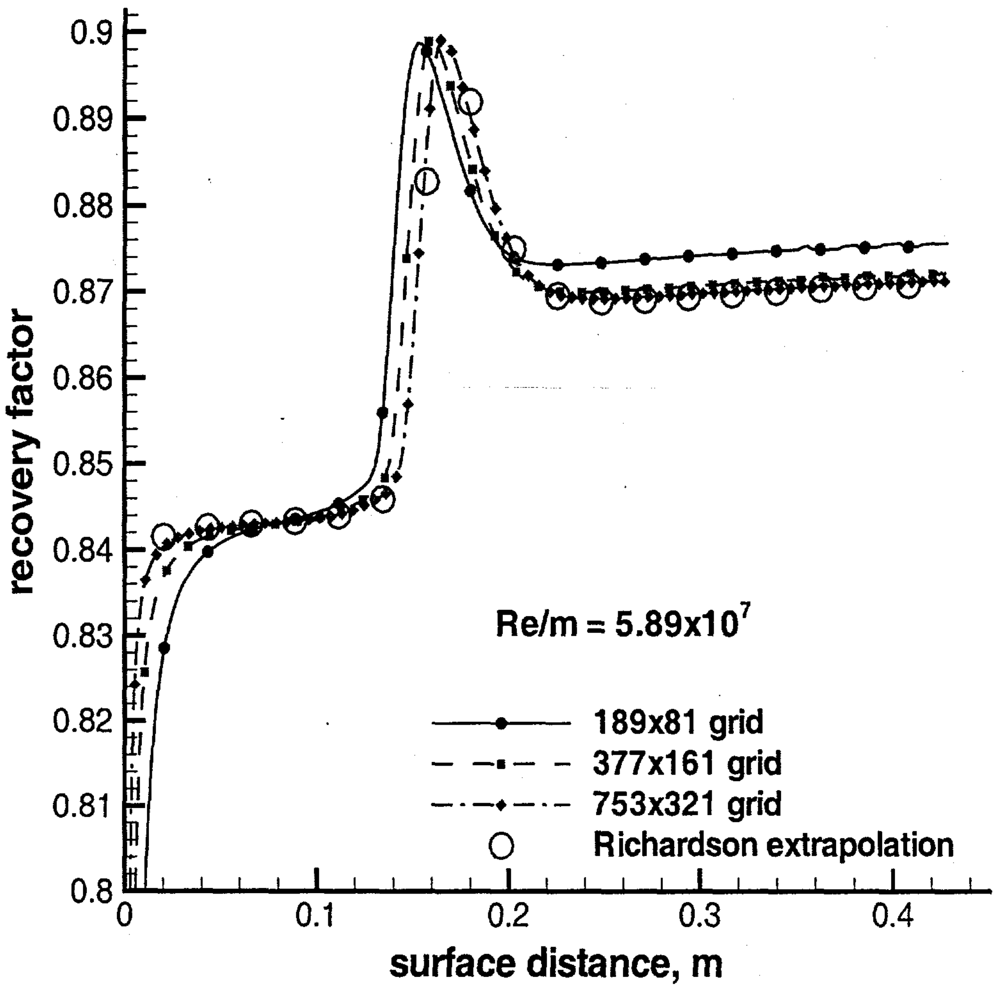

recovery factor
0.9
0.89
0.88
0.87
0.86
0.85
0.84
0.83
0.82
0.81
0.8
0
0.1
0.2
0.3
0.4
surface distance, m
Re/m = 5.89x10⁷
189x81 grid
377x161 grid
753x321 grid
Richardson extrapolation

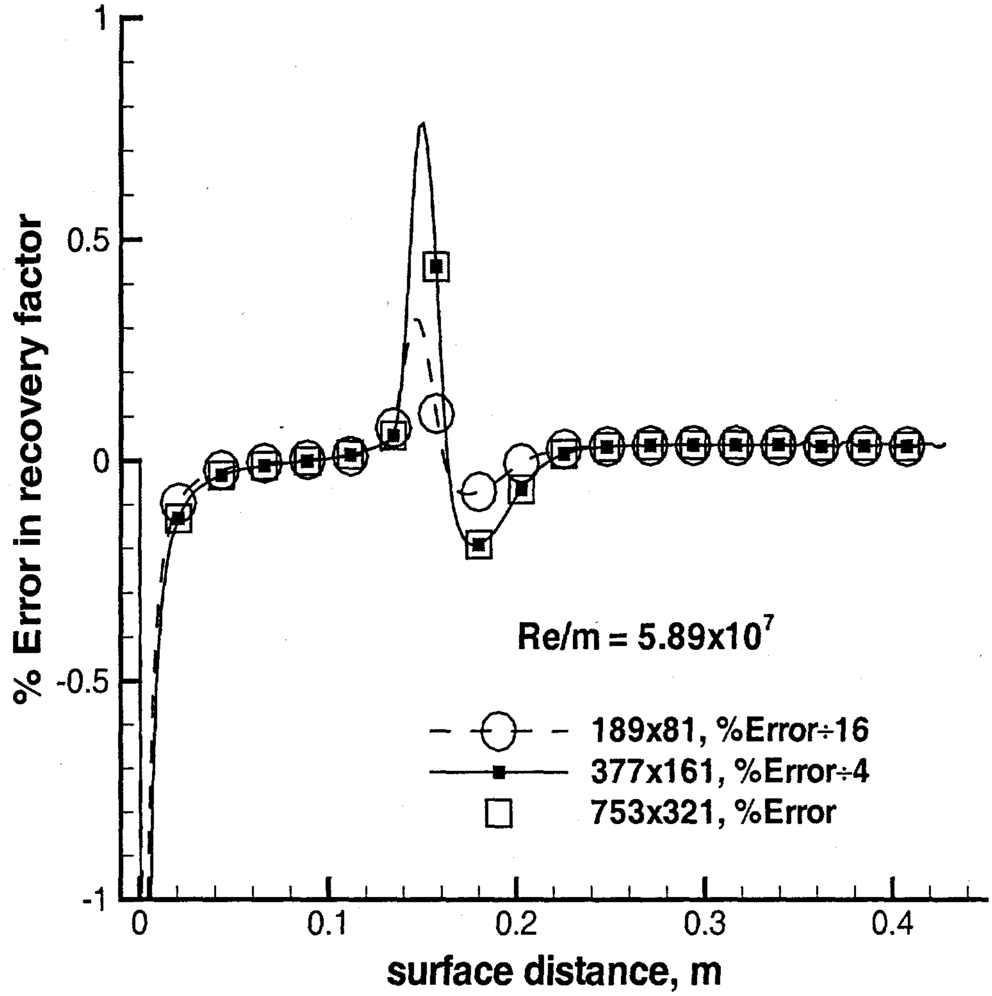

Re/m = 5.89x10^7
189x81, %Error÷16
377x161, %Error÷4
753x321, %Error
% Error in recovery factor
surface distance, m
1
0.5
0
-0.5
-1
0
0.1
0.2
0.3
0.4

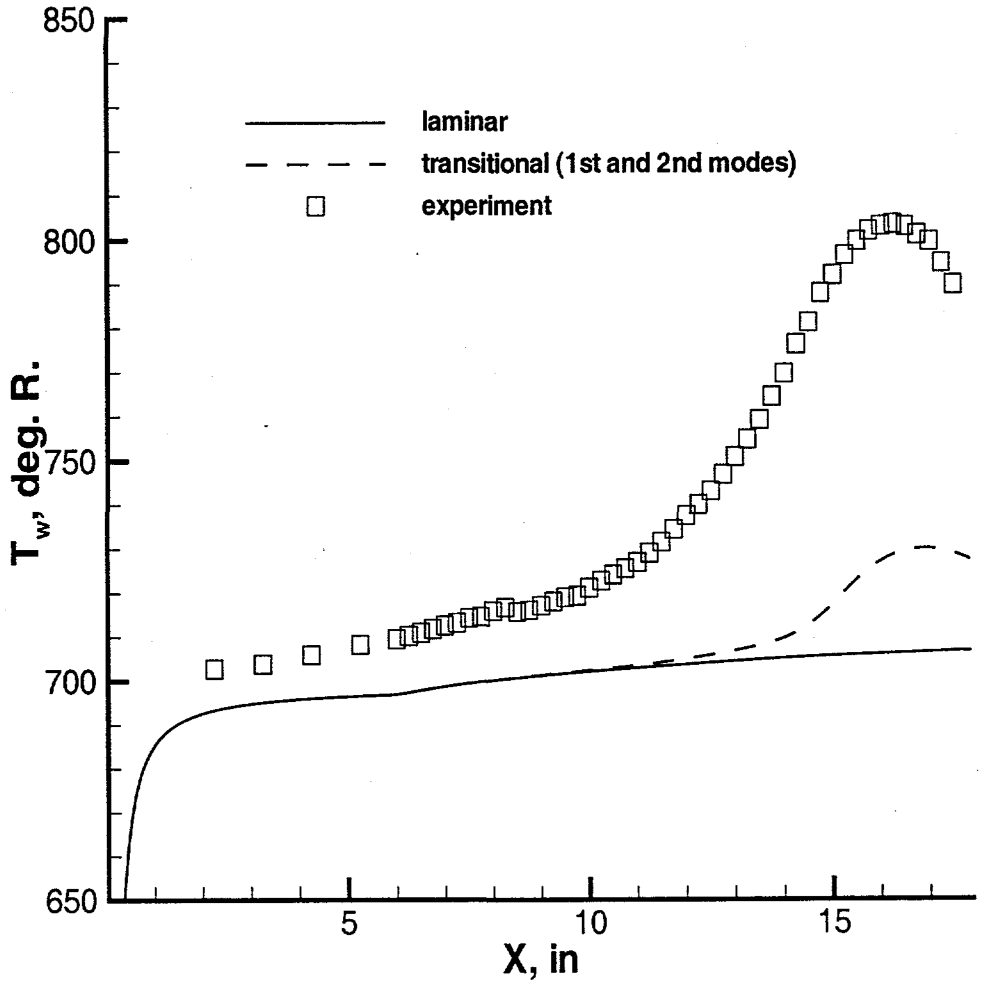
850
800
750
700
650
T_w, deg. R.
5
10
15
X, in
laminar
transitional (1st and 2nd modes)
experiment